Gait Symmetry Analysis with FMCW MIMO Radar

Lopez-Delgado, Ignacio E.; Wang, Dingyang; Fioranelli, Francesco; Grajal, Jesus

DOI
10.1109/TMTT.2025.3542183

Publication date
2025

Document Version
Final published version

Published in
IEEE Transactions on Microwave Theory and Techniques

Gait Symmetry Analysis With FMCW MIMO Radar

Ignacio E. López-Delgado, *Student Member, IEEE*, Dingyang Wang, *Member, IEEE*, Francesco Fioranelli, *Senior Member, IEEE*, and Jesús Grajal, *Senior Member, IEEE*

***Abstract*— Monitoring gait symmetry reliably is crucial, as it is an early indicator of Parkinson's disease (PD). In this work, a method is presented to analyze gait asymmetries using a 24-GHz frequency-modulated continuous-wave (FMCW) multiple-input–multiple-output (MIMO) radar in a nonclinical environment. The proposed method is validated by analyzing the gait of 60 people recorded in an environment that presents multiple challenges such as multipath, gait interruption events, and different trajectories, which cause aspect angle variability. This article presents algorithms to address these challenges to extract useful gait information from the radar data and discusses the performance of the proposed system, analyzing the ratio of correct feet identifications and the accuracy of the asymmetry gait parameters. It achieved a mean absolute error of the symmetry ratio below 8% for all gait parameters. This shows that the proposed system and algorithms are robust for both clinical and in-home implementations.**

***Index Terms*— Frequency-modulated continuous-wave (FMCW) radar, gait analysis, gait symmetry, multiple-input–multiple-output (MIMO) radar, Parkinson's disease (PD).**

I. Introduction

PARKINSON'S disease (PD) is a serious neurodegenerative disorder that has no cure since it is diagnosed when the degree of affection is too high to stop it with current treatments [1]. Therefore, the early detection of PD is critical to apply suitable medications and treatment and, thus, increase the quality of life of patients [2].

Currently, the diagnosis of PD is based on a clinical evaluation carried out by doctors [3]. This evaluation analyzes various biomarkers, such as gait, tremors, or voice changes. Among all the gait biomarkers related to PD, gait asymmetry appears in the early stages of the disease, even before patients seek medical attention [1]. Therefore, the analysis of gait symmetry can greatly help the early detection of PD [4], [5], [6].

It is important to acknowledge that gait analysis should be carried out at home because clinical evaluations are expensive, inevitably sporadic, and time-limited, and people are usually biased during these examinations, i.e., their movements may not be natural [7], [8]. Thus, clinical examinations do not allow a continuous analysis of the progression of the patient. On the contrary, analyzing gait at home can provide a continuous evaluation of each patient.

Among the technological solutions available to analyze gait at home, radar technology is the strongest candidate because it is capable of doing the following [8].

1) *Contactless Analysis:* It is comfortable for the patient, and it does not modify gait, unlike wearable sensors.
2) *Continuous Monitoring:* It is not limited by batteries, unlike wearables. It is not limited by light conditions, unlike video cameras.
3) *Privacy-Preserving Analysis:* Radars do not capture plain images of the subjects analyzed, unlike video cameras.

Considering these advantages, radar technology has been already validated to analyze gait in multiple setups [8], [9], [10], [11], [12], [13], [14], [15], tested in controlled environments [16], [17], [18], [19], [20], and even implemented at home [7], [13], [21], [22]. However, these studies are usually limited to gait paths in the more favorable radial direction with respect to the radar or are focused on gait parameters unrelated to gait symmetry.

Specifically, gait symmetry has not usually been analyzed with radar because of the complexity of feet identification [10], i.e., assigning the different gait parameters to the right and left feet. Even though it is possible to analyze gait symmetry without feet identification [9], [20], the most used and clinically relevant symmetry metrics require this identification. Moreover, analyzing the relationship between the gait symmetry and the foot of dominance is relevant to detect PD [23].

In the existing literature, Wang et al. [10] were the first to propose a method to identify and track the feet to quantify gait asymmetry. However, their method was constrained to a treadmill, where the patient is near the radar, and the feet are the only targets in the field of view.

Hadjipanayi et al. [15] have recently reported symmetry metrics, which use the feet information deploying a three-node radar network. However, they do not provide information on the technique used to associate each cycle with the right and left feet, and it is unclear whether their technique offers enough

Received 30 October 2024; revised 13 January 2025; accepted 11 February 2025. This work was supported by MCIN/AEI/10.13039/501100011033 and NextGenerationEU/PRTR under Grant PID2020-113979RB-C21 and Grant PID2021-128469OB-I00. The work of Ignacio E. López-Delgado was supported in part by FPU Fellowship through Spanish Ministry of Innovation, Science and Universities under Grant FPU20/06405 and Grant EST24/00008. The work of Dingyang Wang and Francesco Fioranelli was supported in part by Dutch Research Council (NWO) through RAD-ART, DARE, and NERD. *(Corresponding author: Ignacio E. López-Delgado.)*

This work involved human subjects in its research. Approval of all ethical and experimental procedures and protocols was granted by TU Delft.

Ignacio E. López-Delgado and Jesús Grajal are with the Information Processing and Telecommunications Center, Universidad Politécnica de Madrid, 28040 Madrid, Spain (e-mail: ie.lopez@upm.es; jesus.grajal@upm.es).

Dingyang Wang and Francesco Fioranelli are with the Microwave Sensing Signals and Systems (MS3) Group, Delft University of Technology, 2628 CD Delft, The Netherlands (e-mail: d.wang-6@tudelft.nl; f.fioranelli@tudelft.nl).

Data is available on-line at https://doi.org/10.4121/7cfe7f4f-e8ef-4a06-8359-ca5831e22810.

Digital Object Identifier 10.1109/TMTT.2025.3542183

resolution to fully differentiate them [15]. Moreover, their gait paths are constrained to straight paths radial to the line of sight of the nodes in their radar network.

This article presents a novel method to analyze gait symmetry using a 24-GHz multiple-input–multiple-output (MIMO) radar. To validate this technique, 60 people are monitored while walking in an indoor setup resembling a home with pieces of furniture and clutter. The participants were asked to perform different tasks, which involved walking with different aspect angles with respect to the radar line of sight. Moreover, the room setup includes the effect of multipath from walls and furniture. The robustness of the technique is comprehensively analyzed as a function of the number of virtual channels of the MIMO radar, the aspect angle, and the multipath impact. Moreover, its performance is compared with other state-of-the-art techniques.

A feet identification accuracy of 94% is achieved in the regions with less significant multipath effect using 15 MIMO channels. This accuracy drops to 70% in the regions with more intense multipath. Moreover, the symmetry ratio of different gait parameters is calculated in all the room regions with an error below 8%, which makes it promising for potential clinical and in-home implementations. In addition, as a further contribution, the recorded radar data are made publicly available online [24].

The rest of this article is structured as follows. Section II introduces the radar used for data collection and the methods implemented to identify the feet from the radar data. In Section III, the experimental setup and protocol, and the validation techniques are presented. Section IV analyzes the results obtained, considering the feet detection accuracy and the gait asymmetry error. Finally, the conclusion of this work is drawn in Section V.

II. Proposed Methods

In this section, the radar used and its configuration are presented (see Section II-A). Moreover, the proposed techniques to analyze gait asymmetry are introduced. First, in Section II-B, the gait parameter extraction is explained. Then, Sections II-C and II-D present two new algorithms to assign each step to the right or left feet. It is important to clarify that the algorithms in Sections II-B–II-D must be executed sequentially. Finally, Section II-E presents the proposed strategies to handle gait interruption events.

A. Radar Device

The 24-GHz MIMO radar Inras Radarbook 2 [25] is selected for this work. The radar operational range and configuration are summarized in Table I. This radar features two transmitters and eight receivers in its MIMO array. Both transmitters operate in frequency-modulated continuous-wave (FMCW) mode in the frequency range of 24–24.25 GHz. They are multiplexed in the time domain, generating frequency bursts of 300 μs in frames of 620 μs (slow time, denoted by τ). This allows capturing velocities below 5 m/s [26], the maximum velocity expected for a human walking.

TABLE I
Radar Operational Parameters and Configuration

Parameter	Operational range	Config.
Number of transmitters	1-2	2
Number of receivers	1-8	8
Number of virtual channels, N_v	15	4, 8, 15
Central frequency f_0 (GHz)	24	24
Bandwidth B (MHz)	0-250	250
Range resolution ΔR (m)	$\geq$ 0.6	0.6
Transmitted power P_{TX} (dBm)	(-20)-(10)	10
Antenna gain G (dB)	13.5	13.5
Sing. elem. elevation beamwidth (°)	10	10
Sing. elem. azimuth beamwidth (°)	80	80
Phased array azimuth beamwidth (°)	$\geq$ 7	7
Interrogation time T_I (μs)	20-9000	620
Max. radial velocity $\nu_{\max}^{\text{rad}}$(m/s)	0.35-150	5
Chirp time T_c (μs)	20-9000	300
Radar-PC commun. interval (s)	0.02-5	5
Sampling rate f_s (ksps)	300-1800	500
Samples per chirp, N	90-540	152
Range (m)	0 - 35	0 - 10

The combination of each transmitter–receiver pair leads to a 15-element virtual phased array whose elements are spaced by $\lambda/2$ (at 24 GHz).[1] When all 15 channels are used, a broadside azimuth resolution of 7° is achieved. As a consequence of the radar's narrow beam in elevation, the radar is located on the ground to analyze the motion of the lower limbs.

Each receiver samples the data at $f_s = 500$ ks/s to explore the area ranging in the first 10 m away from the radar. The sampled data are arranged into a 3-D tensor/cube $\mathbf{s}(t, \tau, \chi)$, whose dimensions are the fast time (t), slow time (τ), and the number of channels (χ). This type of radar data is the starting point for the subsequent developed processing pipeline.

It is important to clarify that the following algorithms can be applied to other MIMO radar modules. In fact, their performance can be improved by moving to higher frequencies, where it is possible to use a wider bandwidth and achieve greater distance resolution.

B. Gait Parameter Extraction

The sampled data, arranged into the aforementioned 3-D cube $\mathbf{s}(t, \tau, \chi)$, are processed, as shown in Fig. 1, and then explained in detail in the following steps.

1) The range information is extracted performing an FFT on $\mathbf{s}(t, \tau, \chi)$ along the fast-time dimension, achieving $\mathbf{S}(R, \tau, \chi)$, where R is the range. Previous to the FFT, $\mathbf{s}(t, \tau, \chi)$ is windowed along the fast-time dimension with a Hann window. The FFT has a length of $4N$ samples.
2) $\mathbf{S}(R, \tau, \chi)$ is high-pass filtered along the slow-time dimension to eliminate the static clutter. A cutoff frequency of 5 Hz is used in this work.
3) The azimuth information is extracted from the FFT of $\mathbf{S}(R, \tau, \chi)$ along the channel direction χ, achieving the range–time–azimuth cube: $\mathbf{S}(R, \tau, \theta)$, where θ denotes

[1]Since there are two transmitters and eight receivers, their combination leads to a 16-element virtual phased array. However, two of these elements overlap for motion compensation purposes, remaining 15 nonoverlapping elements [25].

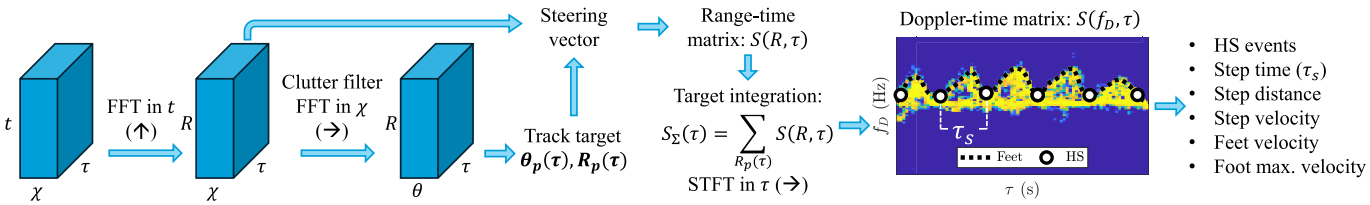

Fig. 1. Proposed algorithms implemented to extract the spatiotemporal gait parameters. The radar signal is processed to extract the Doppler–time matrix, which is then used to extract the HS events and gait parameters.

the azimuth. Previous to the FFT, $\mathbf{S}(R, \tau, \chi)$ is windowed with a Hann window along the virtual channel dimension χ. The FFT has in this case a length of $8N_v$ samples.

4) The range and azimuth location of the target, $R_p(\tau)$ and $\theta_p(\tau)$, are extracted from each time frame of the range–time–azimuth cube implementing a peak detector and a low-pass filter in the slow-time dimension. Multiperson scenarios would require determining first the number of targets and tracking them during this stage. The subsequent algorithms should then be applied for each detected person [27].
5) The range–time matrix, $\mathbf{S}(R, \tau)$, is extracted by multiplying each slow-time frame of $\mathbf{S}(R, \tau, \chi)$ by the steering vector $v(\tau)$, given by

$$v(\tau) = \exp\{-j\pi \sin(\theta_p(\tau))[0, 1, \ldots, N_v - 1]\}. \quad (1)$$

The steering vector is windowed with a Hann window to reduce the sidelobe level.
6) The range bins containing the target signature, $R_p(\tau)$, are coherently integrated to extract $S_\Sigma(\tau)$

$$S_\Sigma(\tau) = \sum_{R_p(\tau)} \mathbf{S}(R, \tau). \quad (2)$$

7) The Doppler–time matrix, $\mathbf{S}(f_D, \tau)$, is extracted performing a short-time Fourier transform (STFT) on $S_\Sigma(\tau)$ with a temporal shift of one sample and a 50-ms Hann window. During this time, it is assumed that the motion of the target does not change. The Doppler axis can be transformed to a radial-velocity axis, v_r, by

$$v_r = \frac{cf_D}{f_0}. \quad (3)$$

8) The step time, τ_s, is the interval between two consecutive heel-strike (HS) events, which are the local minima of the foot velocity [9]. The feet are easily isolated from the Doppler–time matrix because they present the largest velocities [9], as shown in Fig. 1.
9) The step distance is the distance traveled during the step time, both extracted from the range–time–azimuth cube [7]. The step velocity is the step distance divided by the step time.
10) The foot maximum velocity, $v_{\max}$, of each step is finally extracted as

$$v_{\max} = \frac{v_{\max}^{\text{rad}}}{\cos\alpha} \quad (4)$$

where $v_{\max}^{\text{rad}}$ is the maximum of the foot's radial velocity of each step, extracted in Step 8 from the Doppler–time matrix, and α is the aspect angle, i.e., the angle between the radar line of sight and the gait trajectory, both depending on the measurement geometry. For further information, refer to Section III.

This signal processing pipeline extracts the gait parameters used to evaluate gait symmetry: step time, distance and velocity, and foot maximum velocity. Furthermore, the range and azimuth position of the target and the foot velocity are obtained. These parameters are then used to identify the feet as explained in Section II-C.

C. 3SF Feet Identification Algorithm

In this section, the proposed algorithm to identify the feet during gait is presented. The algorithm proposed is based on the fact that during the mid-swing stage, one foot experiences the maximum radial velocity, while the other is still on the ground. This algorithm extracts the range and azimuth of the target with maximum radial velocity during the mid-swing stage, i.e., the footprint of the moving foot. The evolution of these footprints is then analyzed to identify the feet.

The steps carried out to locate the footprints are summarized in Fig. 2 and explained in the following steps. This algorithm is performed for each step interval τ_s, extracted in Step 8 of Section II-B.

1) Extract the Doppler–time–azimuth cube $\mathbf{S}(f_D, \tau, \theta)$: the range bins containing the person signature $R_p(\tau)$ in the range–time–azimuth cube $\mathbf{S}(R, \tau, \theta)$ (extracted in Step 3 of Section II-B) are added; these are seven bins in this case to achieve a span of about 1 m. Then, an STFT is performed along the slow-time domain with a temporal shift of one sample and a 50-ms Hann window.
2) Extract the azimuth of the moving foot, $\theta_f(\tau_m)$: The ten azimuth bins surrounding the person, θ_p, the mid-swing frames, τ_m, and the ten Doppler frequency bins surrounding the foot's Doppler $f_{D,f}$ are selected from the Doppler–time–azimuth cube to obtain $\mathbf{S}(f_{D,f}, \tau_m, \theta_p)$, where the mid-swing frames are the ones in which the foot velocity is above the 95% of its maximum. The foot azimuth estimates $\theta_f(\tau_m)$ are the power peaks of each time frame of $\mathbf{S}(f_{D,f}, \tau_m, \theta_p)$.
3) Extract the range of the moving foot, $R_f(\tau_m)$: the range bins of the person R_p are selected from the range–time matrix (known from Step 5 of Section II-B). An STFT is then performed along the time domain to extract the range–Doppler–time cube, applying a temporal shift of one sample and a 50-ms Hann window. The mid-swing

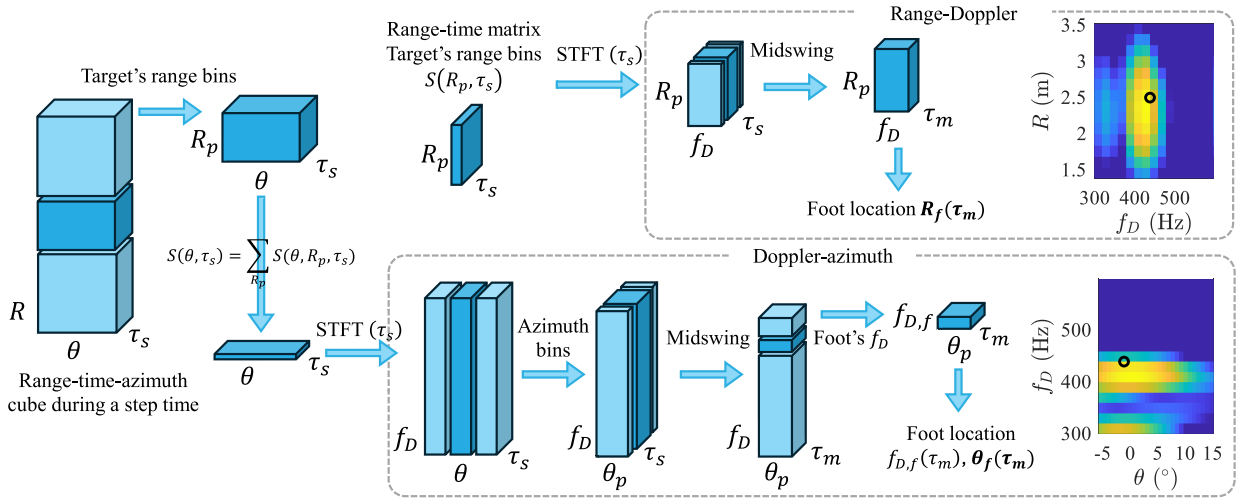

Fig. 2. Proposed algorithms implemented to locate the feet during the mid-swing stage. The range–time matrix and the range–time–azimuth 3-D cube are extracted from Section II-B. The feet are detected from the range–Doppler and the Doppler-azimuth matrices simultaneously.

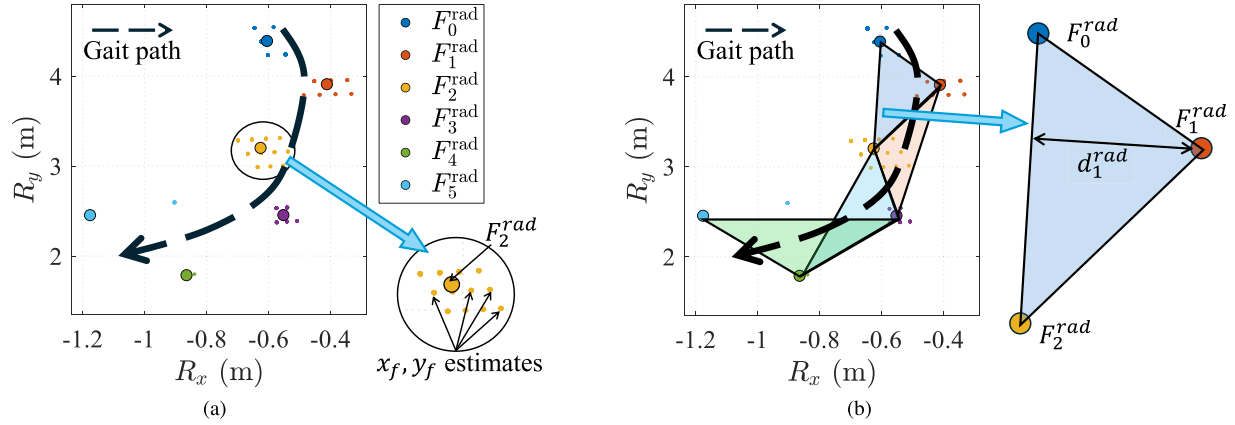

Fig. 3. Proposed 3SF algorithm to identify left and right feet. (a) Footprints corresponding to each step, F_k^{rad}, are estimated from the x_f, y_f estimates, being F_k^{rad} the footprint of the kth step. (b) Triangle is formed out of each of three consecutive footprints to identify the feet.

frames, τ_m, are selected from the range–Doppler–time cube, extracting $\mathbf{S}(R_p, f_D, \tau_m)$. For each time frame of $\mathbf{S}(R_p, f_D, \tau_m)$, it is selected the foot's Doppler frequency bin $f_{D,f}$. The foot range estimates $R_f(\tau_m)$ are the peaks of each time frame of $\mathbf{S}(R_p, f_{D,f}, \tau_m)$.

As a result of the proposed algorithm, a range-azimuth estimate is extracted for each mid-swing time frame, denoted by $R_f(\tau_m)$, $\theta_f(\tau_m)$, respectively. The x_f, y_f coordinates of the moving foot can be obtained as

$$\begin{aligned} x_f &= R_f \cos(\theta_f) \\ y_f &= R_f \sin(\theta_f). \end{aligned} \tag{5}$$

These estimates are represented in Fig. 3 with dots. The location of each footprint is the centroid of each step's estimates, represented in Fig. 3 as a colored circle with the reference label F_k^{rad}, where F_k^{rad} is a column vector with the x, y coordinates of the footprint of the kth step, where $k \in [0, 1, \ldots, K-1, K]$, with K being the number of strides.

A triangle is then shaped from each of three consecutive footprints, as shown in Fig. 3(b). For each footprint F_k^{rad}, where $0 < k < K$, it is calculated the distance between F_k^{rad} and $(F_{k+1}^{\text{rad}} - F_{k-1}^{\text{rad}})$, computed as [28]

$$d_k^{\text{rad}} = \frac{(F_k^{\text{rad}} - F_{k-1}^{\text{rad}})^T \cdot \begin{pmatrix} 0 & 1 \\ -1 & 0 \end{pmatrix} \cdot (F_{k+1}^{\text{rad}} - F_{k-1}^{\text{rad}})}{\| F_{k+1}^{\text{rad}} - F_{k-1}^{\text{rad}} \|} \tag{6}$$

where $\|\cdot\|$ is the norm operator. This distance basically represents the separation from the foot k and the walking trajectory, and it is used to assign the steps to the left and right feet: if $d_k^{\text{rad}} > 0$, the step k is carried out with the right foot. Otherwise, it is carried out with the left foot, as in the example of Fig. 3.

The initial and final steps $k = 0$ and $k = K$ are classified as left or right based on the steps 1 and $K - 1$, respectively. For instance, if step $K - 1$ is a left step, K is a right step.

The reliability of the three-step-footprint (3SF) algorithm is based on the unlikeliness of committing an assignment error since three footprints are used for every decision. Moreover, the algorithm is robust for all gait directions and against erratic paths, as shown in Fig. 3. Still, the 3SF algorithm is limited by the number of steps needed (at least 3) and does not guarantee alternation between the right and left, as normally observed in

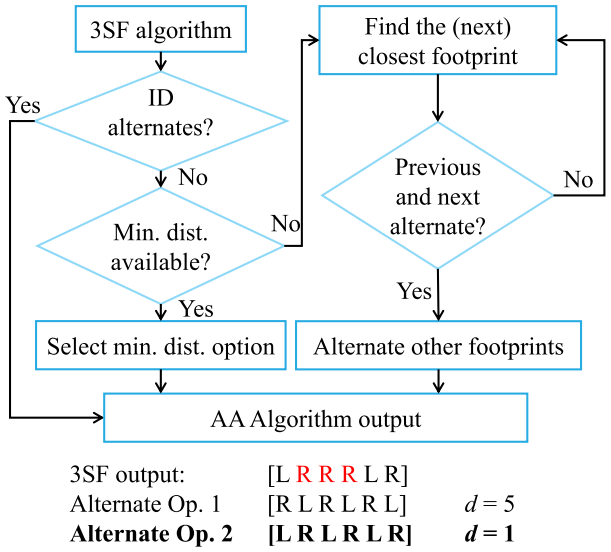

Fig. 4. Proposed AA algorithm, applied for each gait sequence without alternation at the output of the 3SF algorithm. d represents the distance between each alternate option and the 3SF output.

human gait. In Section II-D, a very simple solution to this issue is proposed and explored.

D. AA Feet Identification Algorithm

This section presents an algorithm to correct possible assignment errors of the 3SF algorithm. This approach is based on the fact that human gait normally alternates the foot that carries out each step, i.e., if step k is carried out with the left leg, steps $k-1$ and $k+1$ are carried out with the right leg. The always alternate (AA) algorithm, summarized in Fig. 4, forces to have feet alternation at the output of the 3SF algorithm.

The AA algorithm is applied for every gait sequence (time comprised between the beginning and the end of the gait) without left and right alternations at the output of the 3SF algorithm. An example is shown at the bottom of Fig. 4. The steps of the AA algorithm are given as follows.

1) Compare the two possible alternate options with the 3SF output. The closest alternate option is the output of the AA algorithm.
2) If both alternate options are equally close to the 3SF output, an iterative process is started, checking each step from closest to farthest from the radar. The first step reporting alternation is used to propagate it to the other steps of the considered gait sequence.
3) In the unlikely case that there are no alternations at all, the closest step to the radar is selected, and the other steps of the gait sequence are forced to alternate using this as a reference.

Notably, to apply the AA algorithm, it is critical to isolate gait sequences, as foot alternation is not guaranteed between the last step of a gait sequence and the first step of the following gait sequence. For this reason, an approach for gait interruption detection is needed, as explained in Section II-E.

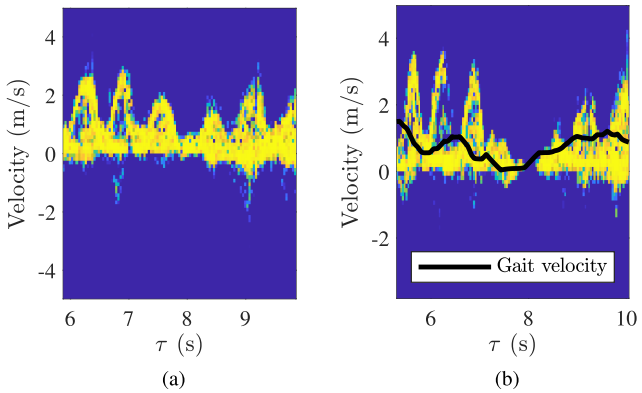

Fig. 5. Example of signatures for short gait interruptions. (a) Foot maximum velocity decay. (b) Gait velocity decay. The gait velocity is represented in black as a reference.

E. Gait Interruption Detection for Gait Sequence Separation

In this section, we present three developed techniques to detect gait interruption events because foot alternation is not guaranteed between gait sequences. The techniques presented in this section are effective at separating the gait sequences in Section III but can be applied to other environments.

The first situation analyzes a person who stops for a long period of time (>1 s). This causes a strong power decay in the range–time and Doppler–time matrices since the clutter-removal filter eliminates the presence of static objects. Under these scenarios, there is no target detected. The first and last time frames in which the target is detected determine the first and last frames of a gait sequence, respectively.

However, when a person interrupts the gait during a short period of time (<1 s), this power decay is not observed. These short gait interruptions can be identified by analyzing the foot maximum velocity and the gait velocity, as shown in Fig. 5.

1) The last and first steps of two consecutive gait sequences sometimes display a smaller foot maximum velocity, as shown in Fig. 5(a). This happens when the last step of a gait sequence ends with both feet under the trunk. These stops are recognized when the maximum velocity of two consecutive gait cycles drops below 70% of the mean foot maximum velocity.
2) When the last step of a gait sequence ends with the feet separated, all gait cycles resemble the normal situation, as shown in Fig. 5(b). Still, the gait velocity drops as a consequence of the gait interruption. These stops are recognized when the gait velocity drops below 60% of the mean gait velocity.

It is more convenient to separate gait sequences by analyzing the foot maximum velocity because a gait cycle is sometimes missed when gait sequences are separated based on the gait velocity.

III. Experimental Setup

This article validates the algorithms presented in Section II by analyzing human gait in a scenario that emulates a home setup with clutter and furniture, as shown in Fig. 6. Each participant is asked to recreate the situation in which they are sitting in their living room when they remember they forgot

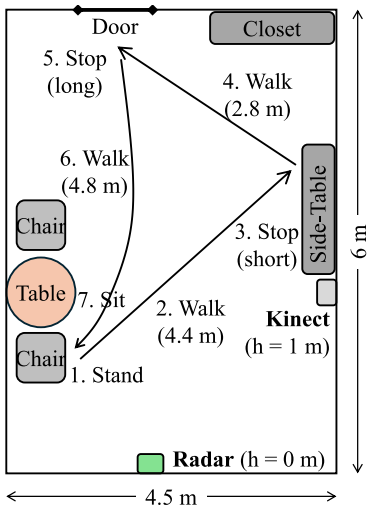

(a)

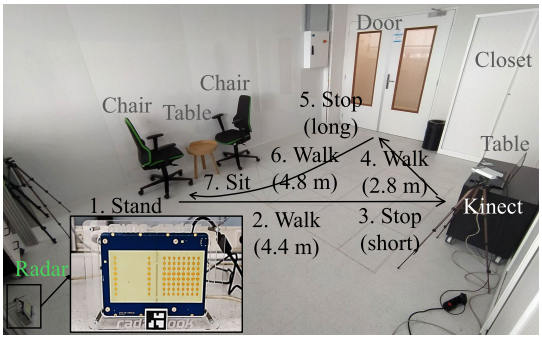

(b)

Fig. 6. Experimental setup with the route walked by the participants and the obstacles present in the room. The radar is located on the floor. The Kinect sensor is 1 m above the floor. (a) Map. (b) Picture.

to lock the door. Thus, they stand up, walk to the side table where the key is, take the key, walk to the door to lock it, and walk back to the chair where they sit down again, as shown in Fig. 6.

The chosen setup presents several challenges.

1) *Aspect Angle Effect:* The radar location is selected to analyze different aspect angles α during the different gait sequences, as shown in Fig. 7.
2) *Multipath Effect:* The gait is recorded in a closed room with the presence of multiple static targets and nearby walls, which increases the complexity of tracking targets.
3) *Gait Interruption Events:* Two different gait interruption situations are forced: a short interruption when taking the key, and a second one, longer, when locking the door.

Examples of the range–time and Doppler–time matrices captured are shown in Fig. 8, where it is possible to observe the phenomena previously described.

1) There is a strong multipath component beyond 6 m caused by the wall at the bottom of the room. This complicates the target detection, especially in the second gait sequence.
2) There are short and long gait interruption events at $\tau = 8$ s and $\tau = 12 - 14$ s, respectively.

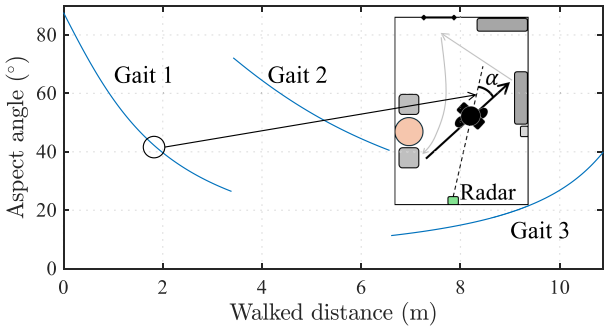

Fig. 7. Aspect angle between the radar and the gait of the person during the route shown in Fig. 6. An example of the aspect calculation is also shown. The discontinuities are caused by the change in the gait directions.

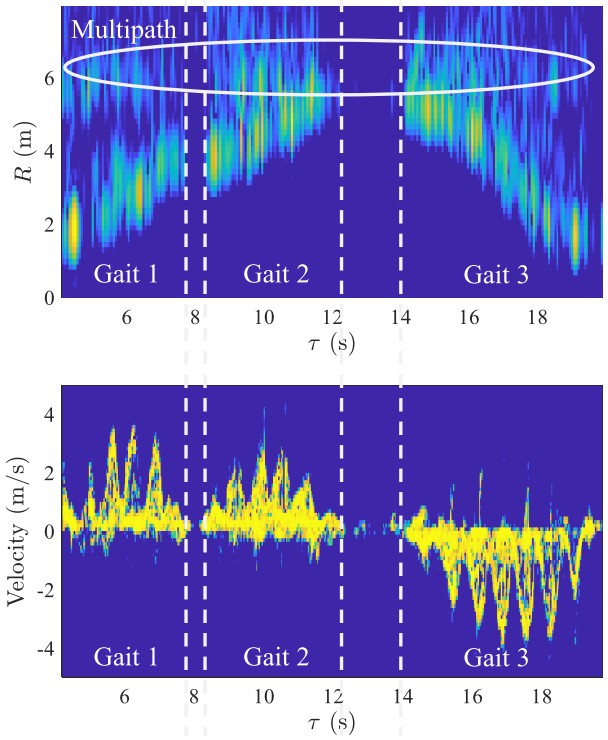

Fig. 8. Example of radar captures of a person performing the experiment presented in this section. Range–time matrix (top). Doppler–time matrix (bottom).

A. Microsoft Kinect Sensor as Ground Truth

The gait recorded with the radar is compared with an Azure Kinect DK camera [29] used as ground truth, which captures image and depth information at 30 ft/s. The Kinect captures are processed with the Azure body tracking SDK implemented through a dedicated Python library [30]. The outputs of this processing pipeline are the xyz location of 32 body parts.

The location of the 32 body parts extracted with the Kinect is low-pass filtered to reduce the noise. The torso location is extracted averaging the pelvis, right hip, left hip, naval spine, chest spine, neck, right clavicle, and left clavicle; the feet locations are extracted averaging the ankles and feet.

The maximum between the left and right foot velocities is selected to extract the foot velocity, which is processed to extract the HS events and the step time and foot maximum velocity, as was done with the radar data. The Kinect torso

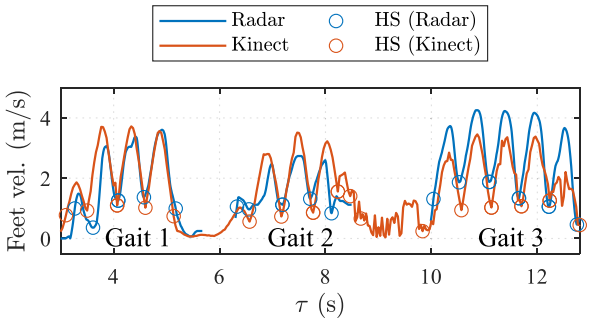

Fig. 9. Comparison of the foot velocity and HS events estimated with the radar and the Kinect. The radar signal is represented only in the time frames where gait is detected.

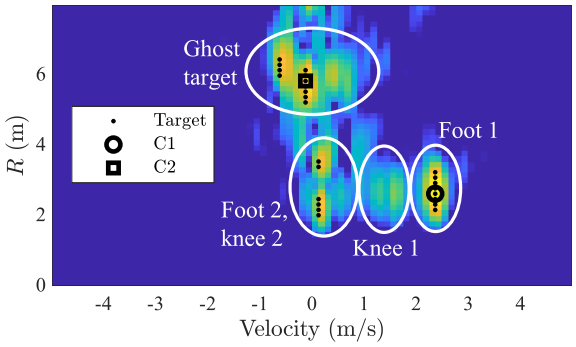

Fig. 10. Example of a range–velocity frame of a person performing the walking experiment shown in Fig. 6. After applying the algorithms proposed in [10], one foot is correctly identified (C1), whereas the other foot is confused with a ghost target (C2).

velocity is combined with the step time to extract the step distance and velocity.

The foot velocity and HS events extracted with the radar and the Kinect are shown in Fig. 9. As shown, there is a high correlation between data from both devices.

Velocity discrepancies are caused by the fact that the radar measures the radial velocity, which decreases for high aspect angles, and the Kinect measures the speed, which is filtered to reduce noise. An undesired effect of this filtering is a reduction in the foot velocity obtained.

Fig. 9 shows that in Gait Sequence 1 (namely, Gait 1 in Fig. 9), where the aspect angle is moderate and the radial velocity measured by the radar is similar to the filtered speed obtained from the Kinect. In Sequence 2, where the aspect angle is higher, the radial velocity is less than the filtered speed. In Sequence 3, where the aspect angle is very small, the radial velocity is larger than the filtered speed.

It is important to take into account that albeit affordable and easy to use, the Kinect is less accurate than other technologies such as infrared cameras or force platforms [8]: Kinect has reported accuracies between 10.4 and 36.7 cm when the person is moving [31], which are worse than radar accuracy metrics [8], [14]. Nonetheless, the experimental conditions required a configurable space with multipath, which is rarely found in laboratories with more accurate benchmarks and ground-truth sensors. Therefore, the Kinect was deemed the most suitable and practical technology despite its lower accuracy.

B. Proposed Algorithm Validation

Besides the proposed algorithms described in Section II, the algorithm proposed by Wang et al. [10] is also implemented in this study to compare the results. In [10], gait asymmetries were analyzed by identifying left and right feet with subjects walking on a treadmill. An eight-virtual channel MIMO radar was placed at one end of the treadmill, facing the participant.

The detections at each time frame were clustered using the range–velocity–azimuth coordinates. The expectation–maximization (EM) clustering algorithm [32], [33] was implemented, as done in [10]: the number of clusters is forced to two, with random initial assignments.

There are some aspects to be considered when applying [10, Algorithms] to the experimental room environment of this article, as shown in Fig. 6.

1) In [10], the radar had only two targets in its field of view: the feet. In this work, there are many targets in the field of view, including ghost targets arising from multipath. Thus, the two clusters are hardly going to correspond directly to the feet. Fig. 10 shows, for example, the targets detected in the range–velocity map using the algorithm presented in [10] and implemented and applied in the setup of Fig. 6. The detections are caused by the feet, knees, and ghost targets. After applying the clustering algorithm, one cluster is located at the moving foot, but the other corresponds to the ghost target.
2) For the implementation of the algorithm proposed by Wang et al. [10], we have decided to assign left or right based on the gait direction. In their proposal, the assignment was done in a simpler way based on azimuth because the gait direction did not change in their experiment, i.e., straight walk on the treadmill.

It is important to take into account that the method proposed by Wang et al. [10] is limited by the measurement setup. Thus, it is expected that the techniques proposed in this work outperform the methods in [10] because the former is specifically designed for an unconstrained environment.

With respect to the work of Hadjipanayi et al. [15], they also analyzed gait asymmetry based on feet identification. Nonetheless, they used a three-node radar network. Since we only use one radar, in this work, their method is not implemented as it would lead to unfair comparisons. Nonetheless, the figures of merit of both techniques are compared.

C. Experimental Protocol

Sixty healthy participants of varying genders, ages, and body types participated in the experiment to validate the proposed algorithms. A summary of the demographics of the participants is shown in Table II.

All the measurements presented in this article are recorded with the approval of the ethics committee of TU Delft. The subjects were informed of the conditions of the experiment and voluntarily agreed to participate. After the experiment,

TABLE II
DEMOGRAPHICS OF THE PEOPLE RECORDED

Gender		**Age**			**Weight** (kg)			**Height** (cm)			**Shoe size**			
F	M	< 30	30-50	> 50	< 70	70-80	> 80	< 170	170-180	> 180	< 40	40-43	> 44	Total
25	35	31	18	11	20	18	22	15	21	24	19	16	25	60

TABLE III
RMSE OF $|\varepsilon_d|$ (cm) FOR THE DIFFERENT GAIT SEQUENCES AND THE NUMBER OF VIRTUAL CHANNELS

N_v	15	8	4
Gait 1 and 3	17	19	35
Gait 2	27	30	47

the data was anonymized, and each participant was assigned to a code.

The participants were asked to repeat three times the protocol shown in Fig. 6, walking as naturally as possible. Consequently, even though all the participants perform the same tasks, each one carries them out uniquely.

The data recorded with the radar, the joint information extracted with the Kinect, and the physiological information of each subject are available online together with the scripts needed to interpret them [24]. The identity of the subjects and the Kinect images are not available for privacy reasons.

IV. RESULTS

The results are analyzed as a function of the number of MIMO virtual channels for azimuth resolution (i.e., 15, eight, and four virtual channels are evaluated) and as a function of the presence of multipath. Specifically, as multipath causes a larger impact on Gait Sequence 2, as shown in Fig. 8, Gait Sequences 1 and 3 are evaluated separately from Sequence 2.

A. Feet Identification Accuracy

First, the reliability of each assignment in the proposed 3SF algorithm is analyzed. Each 3SF triangle is extracted using the radar and the Kinect data separately to compare the distance between the footprint and the gait path extracted with the radar d_k^{rad} and the Kinect d_k^{kin} (as summarized in Fig. 3 for reference). The resulting error is defined as follows:

$$|\varepsilon_d| = \left| d_k^{\text{rad}} - d_k^{\text{kin}} \right|. \tag{7}$$

The RMSE of $|\varepsilon_d|$ is then extracted for the different number of virtual channels and gait sequences. The results are shown in Table III. As a reference, the typical separation between feet is below 30 cm [34]. Thus, an RMSE below this value is needed. From Table III, it can be concluded that the following holds.

1) The RMSE is kept below 30 cm with 15 and eight virtual channels in Gait Sequences 1 and 3 and only with 15 channels in Gait Sequence 2.
2) Gait Sequence 2 (the one with stronger multipath components due to nearby walls) presents a larger error.
3) The error increases as the number of virtual channels decreases, as a consequence of the range and azimuth resolution loss.

Furthermore, the accuracy of the 3SF and AA algorithms is quantified as the ratio between the number of correct identifications and the total number of steps

$$\kappa = \frac{\text{Number of correct identifications}}{\text{Number of steps detected}}. \tag{8}$$

Details of the feet identification accuracy for Gait Sequences 1 and 3 and for Gait Sequence 2 separately are shown in Tables IV and V, respectively. Several conclusions can be extracted from these results.

1) The algorithms proposed in this article outperform the algorithms introduced by Wang et al. [10]. The accuracy of the 3SF + AA algorithms with 15 virtual channels is 0.94, while the accuracy of [10] is 0.53. It is still important to highlight that the performance of [10] is poor because the experiment presented in this article is not conducted on a treadmill.
2) The algorithms proposed in this article are very sensitive to multipath effects, as shown comparing Tables IV and V: the feet detection accuracy drops from 0.94 to 0.7 in the regions with stronger multipath. A similar performance degradation would be expected in multiperson scenarios during the time frames in which different targets are very close to each other.
3) Forcing feet alternation with the proposed AA algorithm improves the results of the 3SF algorithm for all cases studied. This improvement increases with the performance of the 3SF alone, as fewer corrections are needed. For instance, Table IV shows that the overall system performance increases from 0.84 to 0.94 using 15 channels and only from 0.57 to 0.62 using four channels.
4) The algorithms presented are robust for all population groups studied, as no trend can be extracted separating the participants based on demographic information such as age, gender, or body characteristics.

The results show that the radar performance is optimal using all the available 15 MIMO channels. Thus, the gait parameters and symmetry metrics presented in Sections IV-B and IV-C are analyzed only using 15 virtual channels.

B. Gait Parameter Figures of Merit

Before analyzing the asymmetry metrics, it is important to analyze the accuracy of the proposed approach concerning the gait parameter estimation because the asymmetry metrics are derived from the gait metrics. This section presents the absolute value of the relative errors for the different gait parameters $|\varepsilon_r^p|$, calculated as

$$|\varepsilon_r| = \left| \frac{p^{\text{rad}} - p^{\text{kin}}}{p^{\text{kin}}} \right| \tag{9}$$

where p is a gait parameter estimated with both the Kinect and the radar. The gait parameters used to analyze symmetry are

TABLE IV

FEET IDENTIFICATION ACCURACY (κ) OF GAIT SEQUENCES 1 AND 3 (LESS SIGNIFICANT MULTIPATH)

		Gender		**Age**			**Weight** (kg)			**Height** (cm)			**Shoe size**			
Method	N_v	F	M	< 30	30-50	> 50	< 70	70-80	> 80	< 170	170-180	> 180	< 40	40-43	> 44	Total
3SF	15	0.85	0.84	0.85	0.84	0.83	0.85	0.86	0.82	0.84	0.85	0.84	0.86	0.83	0.84	0.84
	8	0.79	0.76	0.79	0.76	0.73	0.78	0.82	0.73	0.80	0.79	0.74	0.79	0.79	0.75	0.77
	4	0.60	0.56	0.58	0.57	0.53	0.58	0.63	0.52	0.58	0.61	0.53	0.60	0.59	0.54	0.57
3SF+AA	15	**0.94**	**0.95**	**0.95**	**0.94**	**0.91**	**0.93**	**0.95**	**0.95**	**0.96**	**0.93**	**0.94**	**0.95**	**0.93**	**0.95**	**0.94**
	8	0.89	0.85	0.87	0.89	0.78	0.91	0.90	0.80	0.92	0.91	0.79	0.90	0.90	0.82	0.86
	4	0.63	0.61	0.63	0.62	0.58	0.62	0.71	0.54	0.62	0.66	0.58	0.64	0.65	0.58	0.62
[10]	15	0.52	0.54	0.52	0.55	0.54	0.53	0.53	0.53	0.53	0.51	0.55	0.54	0.50	0.55	0.53

TABLE V

FEET IDENTIFICATION ACCURACY (κ) OF GAIT SEQUENCE 2 (MORE SIGNIFICANT MULTIPATH)

		Gender		**Age**			**Weight** (kg)			**Height** (cm)			**Shoe size**			
Method	N_v	F	M	< 30	30-50	> 50	< 70	70-80	> 80	< 170	170-180	> 180	< 40	40-43	> 44	Total
3SF	15	0.65	0.62	0.66	0.58	0.59	0.59	0.71	0.60	0.69	0.61	0.61	0.62	0.65	0.62	0.63
	8	0.68	0.63	0.67	0.59	0.65	0.65	0.64	0.64	0.66	0.67	0.61	0.60	0.72	0.62	0.64
	4	0.49	0.51	0.54	0.42	0.50	0.48	0.51	0.51	0.51	0.49	0.50	0.46	0.53	0.50	0.50
3SF+AA	15	**0.72**	**0.70**	**0.75**	**0.63**	**0.67**	**0.67**	**0.77**	**0.67**	**0.81**	0.66	**0.68**	**0.70**	0.74	**0.68**	**0.70**
	8	0.66	0.68	0.73	0.58	0.66	0.66	0.71	0.66	0.66	**0.71**	0.66	0.57	**0.76**	0.67	0.68
	4	0.55	0.49	0.57	0.37	0.50	0.48	0.52	0.52	0.51	0.49	0.52	0.48	0.53	0.51	0.51
[10]	15	0.51	0.53	0.51	0.53	0.53	0.51	0.49	0.56	0.52	0.54	0.50	0.51	0.53	0.52	0.52

TABLE VI

MEAN OF $|\varepsilon_r|$ AS A FUNCTION OF THE ASPECT ANGLE

	0°-30°	30°-60°	60°-90°
Step time	0.05	0.06	0.08
Gait velocity	0.08	0.09	0.15
Step distance	0.12	0.17	0.18
Foot velocity	0.23	0.17	0.19

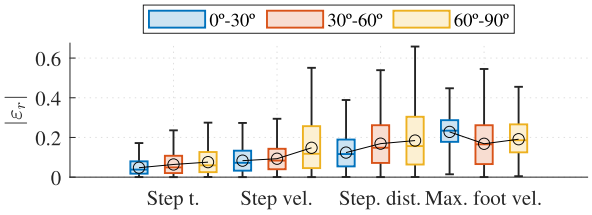

Fig. 11. Distribution of $|\varepsilon_r|$ as a function of the aspect angle between the gait trajectory and the radar line of sight. The mean of $|\varepsilon_r|$ is represented with black circles.

the step time, step velocity, step distance, and foot maximum velocity.

The distribution of $|\varepsilon_r|$ for each gait parameter is shown in Table VI and Fig. 11. Moreover, $|\varepsilon_r|$ is analyzed as a function of the aspect angle between the radar and the gait direction, which is calculated by analyzing the target location extracted with the radar (see Fig. 7). Some conclusions can be drawn from Table VI.

1) The mean $|\varepsilon_r|$ for all gait parameters is below 20%, being below 8% in step time. These errors are above other state-of-the-art contributions [9], [11], [14], probably as a consequence of using the Kinect as reference [31]. Still, the system is accurate enough to analyze gait.
2) The error increases with the aspect angle for all gait parameters except the foot maximum velocity, but this increase is very moderate, allowing gait analysis in all gait directions. In the case of the foot maximum velocity, the error decreases due to a discrepancy of the velocity captured by the Kinect and the radar, as explained in Section III-A.
3) Multiperson scenarios can benefit from accurate gait parameter extraction, as gait parameters can be used to identify people and help separate and track them accordingly [35].

TABLE VII

MEAN OF $|\varepsilon_{SR}|$ OBTAINED IN THIS WORK COMPARED WITH [15]

Parameter	Gait seq. 1 and 3	Gait seq 2	All	[15]
Step time	0.07	0.10	0.06	0.05
Gait velocity	0.06	0.11	0.07	-
Stride distance	0.07	0.13	0.08	-
Foot velocity	0.06	0.11	0.08	-

C. Figures of Merit for Gait Symmetry

The symmetry ratio is the relationship between each mean left and right parameters (step time, step velocity, step distance, and foot maximum velocity), $\overline{p_{\text{left}}}$ and $\overline{p_{\text{right}}}$, for each gait sequence, as follows:

$$\text{SR} = \frac{\overline{p_{\text{left}}}}{\overline{p_{\text{right}}}}. \tag{10}$$

This section reports the absolute error of the symmetry ratio $|\varepsilon_{\text{SR}}|$ and the difference between the symmetry ratio extracted with the radar and the Kinect as follows:

$$|\varepsilon_{\text{SR}}| = |\text{SR}^{\text{rad}} - \text{SR}^{\text{kin}}|. \tag{11}$$

The distribution of $|\varepsilon_{\text{SR}}|$ is shown in Table VII and Fig. 12. The errors reported are below 8% for all the gait parameters considering all sequences.

For comparison, the step time symmetry error reported in [15], comparing the radar metrics with a VICON system, is lower than the one reported in this work. However, this was the only asymmetry metric reported in [15], and it was measured with people walking in an open space (without

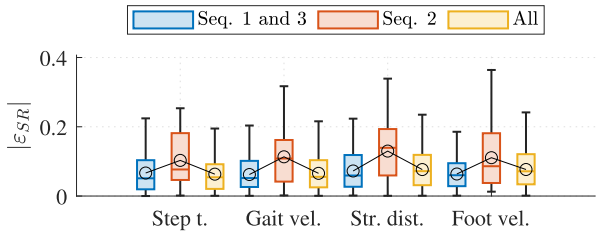

Fig. 12. Distribution of $|\varepsilon_{SR}|$ for the different gait parameters considering the multipath effect: small for Gait Sequences 1 and 3 and strong for Gait Sequence 2. The mean of $|\varepsilon_{SR}|$ is represented with black circles.

multipath) in the radar's radial direction. The results presented in this section show that the proposed system and algorithms are capable of accurately computing symmetry gait parameters in all room regions.

To meet the requirements for PD diagnosis, a mean $|\varepsilon_{SR}|$ below 0.05 would be ideal [4], [5], [6]. While the results shown in Table VII and Fig. 12 are close to meeting these standards, they fall short of this threshold. Nonetheless, the system accuracy may be underestimated due to the use of the Kinect as a reference, suggesting that further validation with more accurate reference systems could provide a clearer understanding of the proposed system's potential for PD detection.

V. Conclusion

This article presents the development of novel algorithms for gait symmetry analysis using a single MIMO radar operating in the 24-GHz band. The proposed algorithms have been validated by analyzing the gait recordings of 60 participants. These data have been collected in an indoor environment with clutter and multipath and have been gathered into a database publicly available online [24].

An azimuth angular resolution of 7°, achieved with 15 MIMO virtual channels, is needed to obtain a feet detection accuracy of 94% in the regions of less significant multipath. This value drops to 70% in the regions with stronger multipath due to nearby walls. Under this configuration, the symmetry ratio errors fall below 8% for all gait parameters.

Based on the results demonstrated in this work, it is shown that MIMO radars are capable of analyzing gait symmetry in a nonintrusive way and in realistic environments, which can help toward technologies for early detection of PD.

Data Availability Statement

The dataset is available under the DOI: 10.4121/7cfe7f4f-e8ef-4a06-8359-ca5831e22810 at the reference: López-Degado, Ignacio Esteban; Wang, Dingyang; Fioranelli, Francesco; and Grajal, Jesús (2024): dataset of human gait in a domestic setup collected with an LFMCW MIMO radar. 4TU.ResearchData dataset: https://doi.org/10.4121/7cfe7f4f-e8ef-4a06-8359-ca5831e22810

Acknowledgment

The authors would like to thank the participants in the experiment for their availability.

References

[1] E. Giannakou, S. Fotiadou, V. Gourgoulis, G. Mavrommatis, and N. Aggelousis, "A comparative analysis of symmetry indices for spatiotemporal gait features in early Parkinson's disease," *Neurol. Int.*, vol. 15, no. 3, pp. 1129–1139, Sep. 2023.

[2] R. Di Paola and R. J. Uitti, "Early detection of Parkinson's disease," *Drugs Aging*, vol. 9, no. 3, pp 159–168, Sep. 1996.

[3] E. Tolosa, A. Garrido, S. Scholz, and W. Poewe, "Challenges in the diagnosis of Parkinson's disease," *Lancet Neurol.*, vol. 20, no. 5, pp. 385–397, 2021.

[4] J. Seuthe et al., "Gait asymmetry and symptom laterality in Parkinson's disease: Two of a kind?" *J. Neurol.*, vol. 271, no. 7, pp. 4373–4382, Jul. 2024.

[5] R. Baltadjieva, N. Giladi, L. Gruendlinger, C. Peretz, and J. M. Hausdorff, "Marked alterations in the gait timing and rhythmicity of patients withde novo Parkinson's disease," *Eur. J. Neurosci.*, vol. 24, no. 6, pp. 1815–1820, Sep. 2006.

[6] M. H. Faria, L. Simieli, S. Rietdyk, T. Penedo, F. B. Santinelli, and F. A. Barbieri, "(A)symmetry during gait initiation in people with Parkinson's disease: A motor and cortical activity exploratory study," *Frontiers Aging Neurosci.*, vol. 15, Apr. 2023, Art. no. 1142540.

[7] Y. Liu et al., "Monitoring gait at home with radio waves in Parkinson's disease: A marker of severity, progression, and medication response," *Sci. Translational Med.*, vol. 14, Sep. 2022, Art. no. eadc9669.

[8] S. Z. Gurbuz, M. M. Rahman, Z. Bassiri, and D. Martelli, "Overview of radar-based gait parameter estimation techniques for fall risk assessment," *IEEE Open J. Eng. Med. Biol.*, vol. 5, pp. 735–749, 2024.

[9] A. Seifert, M. G. Amin, and A. M. Zoubir, "Toward unobtrusive in-home gait analysis based on radar micro-Doppler signatures," *IEEE Trans. Biomed. Eng.*, vol. 66, no. 9, pp. 2629–2640, Sep. 2019.

[10] D. Wang, J. Park, H.-J. Kim, K. Lee, and S. H. Cho, "Noncontact extraction of biomechanical parameters in gait analysis using a multi-input and multi-output radar sensor," *IEEE Access*, vol. 9, pp. 138496–138508, 2021.

[11] K. Saho, K. Shioiri, S. Kudo, and M. Fujimoto, "Estimation of gait parameters from trunk movement measured by Doppler radar," *IEEE J. Electromagn., RF Microw. Med. Biol.*, vol. 6, no. 4, pp. 461–469, Dec. 2022.

[12] R. Soubra, F. Mourad-Chehade, and A. Chkeir, "Automation of the timed up and go test using a Doppler radar system for gait and balance analysis in elderly people," *J. Healthcare Eng.*, vol. 2023, pp. 1–15, Jun. 2023.

[13] P. Siva et al., "Automatic radar-based step length measurement in the home for older adults living with frailty," *Sensors*, vol. 24, no. 4, p. 1056, Feb. 2024.

[14] C. Hadjipanayi et al., "Remote gait analysis using ultra-wideband radar technology based on joint range-Doppler-time representation," *IEEE Trans. Biomed. Eng.*, vol. 71, no. 10, pp. 2854–2865, Oct. 2024.

[15] C. Hadjipanayi, M. Yin, and T. G. Constandinou. (2024). *Capturing Gait Parameters During Asymmetric Overground Walking Using Ultra-wideband Radars: A Preliminary Study*. BioRxiv. [Online]. Available: https://www.biorxiv.org/content/early/2024/07/04/2024.07.01.601550

[16] H. Abedi, J. Boger, P. P. Morita, A. Wong, and G. Shaker, "Hallway gait monitoring system using an in-package integrated dielectric lens paired with a mm-wave radar," *Sensors*, vol. 23, no. 1, p. 71, Dec. 2022.

[17] S. Z. Gurbuz, E. Kurtoglu, M. M. Rahman, and D. Martelli, "Gait variability analysis using continuous RF data streams of human activity," *Smart Health*, vol. 26, Dec. 2022, Art. no. 100334.

[18] R. Veld, A. B. J. Kokkeler, A. Chiumento, and Y. Miao, "Height-adaptive human gait model through radar-driven pipeline with two co-located mmWave MIMO radars," *IEEE Access*, vol. 12, pp. 7199–7223, 2024.

[19] X. Zeng, H. S. L. Báruson, and A. Sundvall, "Walking step monitoring with a millimeter-wave radar in real-life environment for disease and fall prevention for the elderly," *Sensors*, vol. 22, no. 24, p. 9901, Dec. 2022.

[20] S. Ahmed, Y. Seo, and S. H. Cho, "Gait asymmetry evaluation using FMCW radar in daily life environments," in *Bioinformatics and Biomedical Engineering*. Berlin, Germany: Springer, 2023, pp. 116–127.

[21] Z. Sun, Z. Yu, Q. Wang, Z. Wang, B. Guo, and H. Zhang, "CovertEye: Gait-based human identification under weakly constrained trajectory," *IEEE Trans. Mobile Comput.*, vol. 23, no. 5, pp. 5558–5570, May 2024.

[22] H. Abedi, A. Ansariyan, P. P. Morita, J. Boger, A. Wong, and G. Shaker, "In-home cluttered environment gait analysis using mm-wave radar," in *IEEE MTT-S Int. Microw. Symp. Dig.*, Jun. 2024, pp. 42–44.

[23] A. van der Hoorn, A. L. Bartels, K. L. Leenders, and B. M. de Jong, "Handedness and dominant side of symptoms in Parkinson's disease," *Parkinsonism Rel. Disorders*, vol. 17, no. 1, pp. 58–60, 2011.

[24] I. E. López-Delgado, D. Wang, F. Fioranelli, and J. Grajal, "Dataset of human gait in a domestic setup collected with an LFMCW MIMO radar," *4TU.ResearchData*, Oct. 2024, doi: 10.4121/7cfe7f4f-e8ef-4a06-8359-ca5831e22810.v2.
[25] Inras, *AN24-02 ADF24 FMCW Basics*, Inras GmbH, Linz, Austria, 2015.
[26] I. E. López-Delgado et al., "Mm-wave wireless radar network for early detection of Parkinson's disease by gait analysis," in *Proc. IEEE Radar Conf.*, May 2023, pp. 1–6.
[27] D. Wang, F. Fioranelli, and A. Yarovoy, "Quantitative assessment of people tracking with FMCW MIMO radar," in *Proc. 21st Eur. Radar Conf. (EuRAD)*, Sep. 2024, pp. 380–383.
[28] J. P. Ballantine and A. R. Jerbert, "Distance from a line or plane to a point," *Amer. Math. Monthly*, vol. 59, no. 4, pp. 242–243, Apr. 1952.
[29] *Azure Kinect DK*, Microsoft, Redmond, WA, USA, 2024.
[30] I. G. Fernandez. *PyKinectAzure*. Accessed: Sep. 30, 2024. [Online]. Available: https://github.com/ibaiGorordo/pyKinectAzure
[31] T. Wei, B. Lee, Y. Qiao, A. Kitsikidis, K. Dimitropoulos, and N. Grammalidis, "Experimental study of skeleton tracking abilities from Microsoft Kinect non-frontal views," in *Proc. 3DTV-Conf.*, Lisbon, Portugal, Jul. 2015, pp. 1–4.
[32] S. N. Kadir, D. F. M. Goodman, and K. D. Harris, "High-dimensional cluster analysis with the masked EM algorithm," 2013, *arXiv:1309.2848*.
[33] M.-S. Yang, C.-Y. Lai, and C.-Y. Lin, "A robust EM clustering algorithm for Gaussian mixture models," *Pattern Recognit.*, vol. 45, no. 11, pp. 3950–3961, Nov. 2012.
[34] S. Schmidle, A. C. de Crignis, M. Stürzer, J. Hermsdörfer, K. Jahn, and C. Krewer, "Influence of stance width on standing balance in healthy older adults," *J. Neurol.*, vol. 269, no. 12, pp. 6228–6236, Dec. 2022.
[35] Z. Chen, G. Li, F. Fioranelli, and H. Griffiths, "Personnel recognition and gait classification based on multistatic micro-Doppler signatures using deep convolutional neural networks," *IEEE Geosci. Remote Sens. Lett.*, vol. 15, no. 5, pp. 669–673, May 2018.

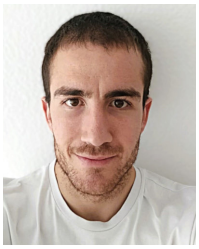

Ignacio E. López-Delgado (Student Member, IEEE) was born in Madrid, Spain, in 1998. He received the B.Eng. degree in telecommunication engineering and the M.Sc. degree in signal theory and communications, under the RF systems track, from the Universidad Politécnica de Madrid (UPM), Madrid, in 2020 and 2021, respectively, where he is currently pursuing the Ph.D. degree at the Information Processing and Telecommunications Center, with a Formación de Profesorado Universitario scholarship granted by the Spanish Ministry of Innovation, Science and Universities.

He has authored four peer-reviewed publications. His research interests include the development of radar systems for gait monitoring and radar signal processing.

Dingyang Wang (Member, IEEE) received the B.S. degree in electronic engineering from Andong National University, Andong-si, Gyeongsangbuk-do, South Korea, in 2015, and the Ph.D. degree in gait analysis from Hanyang University, Seoul, South Korea, in February 2022, with MIMO radar under the supervision of Prof. Sung Ho Cho.

After that, he joined the Radar Computing Laboratory with a joint M.S. and Ph.D. Program, Hanyang University. Since April 2023, he has been a Post-Doctoral Researcher with the Microwave Sensing, Signals and Systems (MS3) Group, Faculty of Electrical Engineering, Delft University of Technology, Delft, The Netherlands. His research includes radar signal processing and multitarget tracking.

Francesco Fioranelli (Senior Member, IEEE) received the Laurea (B.Eng., cum laude) and Laurea Specialistica (M.Eng., cum laude) degrees in telecommunication engineering from the Università Politecnica delle Marche, Ancona, Italy, in 2007 and 2010, respectively, and the Ph.D. degree from Durham University, U.K., in 2014.

He is currently an Associate Professor with TU Delft, Delft, The Netherlands. He was a Research Associate at University College London, London, U.K., from 2014 to 2016, and an Assistant Professor at the University of Glasgow, Glasgow, U.K., from 2016 to 2019. He has authored over 190 peer-reviewed publications and edited the books titled *Micro-Doppler Radar and Its Applications* and *Radar Countermeasures for Unmanned Aerial Vehicles* published by IET-Scitech in 2020. His research interests include the development of radar systems and automatic classification for human signatures analysis in healthcare and security, drone and UAV detection and classification, automotive radar, wind farms, and sea clutter.

Dr. Fioranelli received four best paper awards and the IEEE AESS Fred Nathanson Memorial Radar Award in 2024.

Jesús Grajal (Senior Member, IEEE) was born in Toral de los Guzmanes (León), Spain, in 1967. He received the B.Eng. degree in telecommunications engineering and Ph.D. degrees from the Universidad Politécnica de Madrid, Madrid, Spain, in 1992 and 1998, respectively.

Since 2017, he has been a Full Professor with the Signals, Systems, and Radio Communications Department, Universidad Politécnica de Madrid, Madrid, Spain. His research interests include hardware design for radar systems, radar signal processing, and broadband digital receivers for radar and spectrum surveillance applications.

Dr. Grajal was a corecipient of the 2013 EuCAP Best Antenna Design Paper Award.